Experimental and Numerical Investigation of Ice Crystal Icing on a Heatable NACA0012 Airfoil

Yasir Malik, Lokman Bennani, Alexandros Vorgias, Pierre Trontin, Philippe Villedieu

Experimental and Numerical Investigation of Ice Crystal Icing on a Heatable NACA0012 Airfoil

Yasir A. Malik*, Lokman Bennani†, Alexandros, E. J. Vorgias‡, Pierre Trontin§, Philippe Villedieu¶

Experimental and numerical study is carried out to quantify the accretion growth resulting from ice crystal icing (ICI) on a heatable NACA0012 model. Experiments are performed in the Braunschweig icing wind tunnel encompassing extensive variation of influential parameters such as the supplied heat flux, ice water content, flow velocity, tunnel wet bulb temperature and angle of attack of the test article. Investigations reveal that accretion severity tends to increase for positive wet bulb temperature and the time required for accretion inception reduces with increasing ice water content. Increase in flow velocity tends to have an eroding effect on the accreting ice layer, with accretion shapes shifting from mushroom to conical under the influence of aerodynamic stresses. For negative wet bulb temperatures, increase in supplied heat flux for higher ice water content tends to result in higher accretion growth rates. For constant ice water content and increasing heat flux the cooling power generated from icing cloud is insufficient and takes longer to overcome high temperature gradients resulting in longer accretion inception time. Lastly, upon increasing the angle of attack of the model, the stagnation point shifts to allow for lower tangential aerodynamic stresses on accreted ice layer which leads to increase in icing severity. Experimental results are used to calibrate and validate the numerical models developed at ONERA. The simulations are performed in a two dimensional framework. The unsteady accretion solver is based on an enthalpy approach. An empirical model is used to compute the sticking efficiency. Concerning the phenomenon of erosion, it is taken into account using previously derived models. A heat conduction solver is used to simulate the unsteady thermal behavior of the NACA0012 airfoil. Both solvers are coupled thanks to a Robin-Robin Schwarz method. Initial comparison of accretion growth rates and time of accretion initiation shows good agreement across a wide range of parametric variation.

I. Nomenclature

AoA	=	Angle of attack of the test article
V_{flow}	=	Flow velocity
IWC	=	Ice water content
T_{wb}	=	Tunnel wet bulb temperature
$\dot{q}$	=	Heat flux
IWT	=	Icing wind tunnel
IGS	=	Ice crystal generation system
ICI	=	Ice crystal icing
SDI	=	Supercooled droplet icing
$TUBS$	=	Technische Universität Braunschweig
$ONERA$	=	Office National d'Etudes et de Recherches Aérospatiales
MUSIC-haic	=	MUltidisciplinary tools for the Simulation of In-flight iCing due to High Altitude Ice Crystals

*PhD Researcher, TU Braunschweig, Institute of Fluid Mechanics, Hermann Blenk Str. 37, Germany, y.malik@tu-braunschweig.de
†Research Engineer, ONERA, The French Aerospace Lab, F-31055, Toulouse, France, lokman.bennani@onera.fr
‡Master Student, TU Berlin, Institute of Aeronautics & Astronautics, Marchstraße 12, 10587 Berlin, Germany, e.vorgias@campus.tu-berlin.de
§Research Engineer, ONERA, The French Aerospace Lab, F-31055, Toulouse, France, pierre.trontin@onera.fr
¶Director, DMPE, ONERA, The French Aerospace Lab, F-31055, Toulouse, France, philippe.villedieu@onera.fr

II. Introduction

AIRCRAFT icing has been a source of major flight safety and operability issue since the beginning of aeronautical engineering [1]. A total of 153 engine power loss events on a variety of airplane and engine types have been attributed to engine icing since 1988. This has resulted in surge, stall, rollback or flameout of engines at high altitudes in different regions of the world [2]. A joint worldwide effort is currently underway to further our understanding of the icing phenomenon, develop predictive capabilities and derive effective mitigation means through projects such as MUSIC-haic.

One of the hazards in aviation industry that was long over-looked is ice crystal icing (ICI) which mostly occurs in strongly convective weather, where high concentrations of moisture are lifted to high altitudes. Water is found in different aggregation states and geometrical formations in the atmosphere of Earth [3–5]. Due to no ice accretion on airframe and little turbulence, the conditions associated with ice crystal icing (ICI) often appear benign to pilots [6]. Unlike supercooled droplet icing (SDI), ice crystal icing occurs inside aircraft's engine and on external heated surfaces, such as heated stagnation pressure probes. In the engine, the ice crystals partially melt due to increasing temperature inside the engine compressor which allows the incoming icing cloud to stick to the surface and leads to formation of ice layer which if detached from the surface leads not only to damage of the internal engine parts but also flameout in the combustion chamber. In order to fully understand the ice accretion phenomenon, it is of paramount importance to focus on the qualitative as well as quantitative description of ice accretion growth under a wide range of parametric variation which is the focus of this research work. Key influential parameters based on previous experimental and numerical investigations have been identified to define a test matrix and dedicated experiments on a heatable NACA0012 airfoil have been performed in the Braunschweig Icing Wind Tunnel to provide a large database for calibration and validation of numerical models developed at ONERA. Key outputs presented as part of analysis include quantitative data on accretion thickness, area, volumetric estimation and the instant at which ice accretion begins. The analysis provides new and interesting insights with regards to parameters that play most influential role in initiation of ice accretion that contribute to icing severity or lack thereof. Particular emphasis is paid on experimental and numerical comparison of ice accretion shapes, ice accretion growth rate and the instant of ice accretion initiation for a wide range of parametric variation.

III. Experimental Method

The experimental setup consists of an icing wind tunnel encompassing ice crystal generation and conveyance mechanism, a heatable NACA0012 profile with embedded heaters, temperature and pressure sensors and optical observation system. Additionally, an ice detection software with a user-friendly interface is programmed in Python to post-process the videos using Shadowgraphy technique to provide accretion growth data.

A. Ice Crystal Generation and Conveyance Mechanism

All the experimental results presented in this paper were by-product of experiments performed at the Icing Wind Tunnel (IWT) of TU Braunschweig. An elaborate overview of the the testing facility with details concerning design, construction and commissioning of the wind tunnel is previously documented by Bansmer et al. [7]. Fig. 1 b) provides pictorial illustration of the TU Braunschweig Icing Wind Tunnel facility highlighted in dark blue colour. The tunnel is closed loop with flow velocities reaching up to 40 m/s in a test section with cross-sectional area of 500 × 500 mm. Static temperature inside the tunnel can be maintained in the range of -20 °C to 30 °C. Tunnel cooling is maintained through a dedicated cooling mechanism highlighted in the right most corner of Fig. 1.

Ice crystals are generated inside a cooling chamber wherein the generation, dosing, sieving and finally transport of the ice crystals to the wind tunnel test section takes place. The cooling chamber has a dedicated cooling unit of its own with the capability of ensuring glaciated ice crystals into the wind tunnel by means of an after-cooler. The temperature inside the cooling chamber is kept to -15 °C. The schematics of the IGS is depicted in Fig. 1 a). The ice crystal generation system enables variation in the ice water content in the range of 3 to 20 g/m^3 inside the test section. By means of Cranfield University Isokinetic probe, the CIRA high speed imaging probe and a particle collection tube system the calibration of icing cloud inside the test section was carried out. Cloud characterization lead to a median mass diameter (MMD = D_{50}) of 80 µm, where D_{10} and D_{90} represented the 10% and 90% of the cumulative mass as 20 µm and 220 µm respectively [7, 8]. Cloud chamber technology is employed to simulate the natural occurring ice crystal generation process in atmospheric clouds. As depicted in the top left corner of Fig. 1 a), inside the cooling chamber atomized water droplets are fed through an airstream into balloons where they mix with cooled airstream. Pressure impulse is generated inside the balloons that leads to droplets being frozen leading to growth of naturally shaped ice crystals, using the ambient vapor and liquid droplets [9, 10]. Once ice crystals reach a critical size, they settle into the

bottom of the freezer from where they are later dosed and sieved towards the test section in the form of an icing cloud.

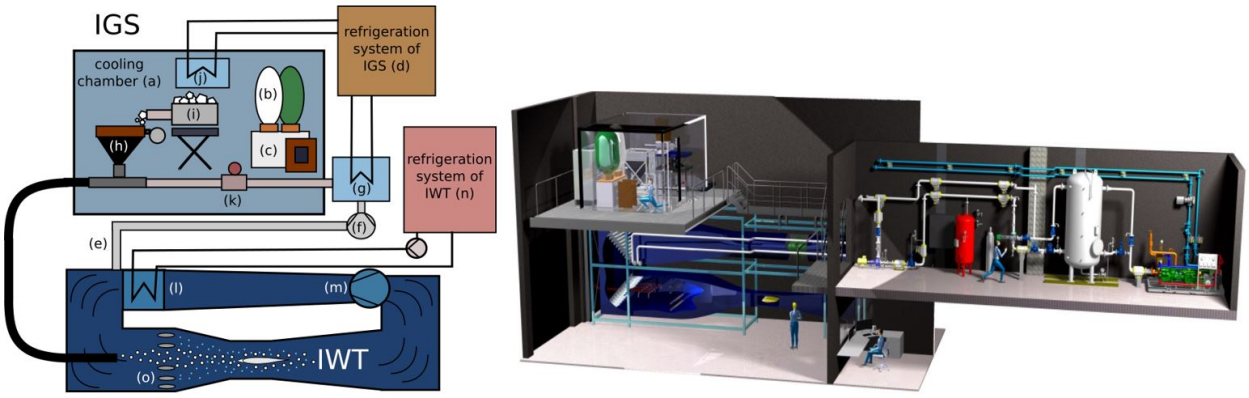

Fig. 1 a) Schematics of IWT and IGS (Left). b) Overview of Braunschweig Icing Wind Tunnel (Right). [7, 8]

B. Test Article and Optical Setup

The test article used for carrying out the experiments is a heatable NACA0012 airfoil. The middle insert of the test article was produced by the National Research Council of Canada (CNRC) with a chord length of 416.56 *mm* and span of 93 *mm*. Fig. 2 b) shows the cross-sectional details of the leading edge of NACA0012 airfoil. The article is embedded with film heaters able to reach heat wattage density up to 30 Watts/inch^2. To prevent heat loss inside the model, an insulation is added which allows the heat flux to travel in the pre-dominant direction i.e. towards the crystals impinging at the aluminium leading edge. An aluminum dissipation insert is inserted to enable uniform heating of the leading edge, with uniformity within the range of ±0.5 °C. Seven type T thermocouples are embedded inside the model for temperature monitoring located between aluminum dissipation insert and the insulation. The aft body of the middle insert is produced from a 3D-printed polymer whereas the leading edge is a heatable aluminium insert.

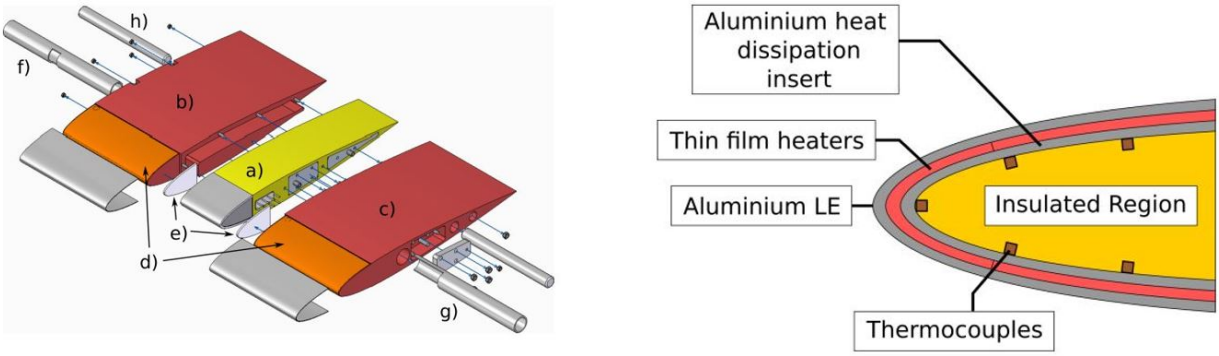

Fig. 2 a) NACA0012 Exploded View (Left). b) Cross-sectional details of L.E. of NACA0012 model (Right).

The idea of the middle insert produced by CNRC was to allow wind tunnel inter-comparison across the world under similar boundary conditions to study the influence of different ice crystal generation mechanism on ice accretion phenomenon. However, to adapt this test article to individual test facilities side parts had to be designed and processed at Technical University of Braunschweig. To that end, as shown in left side of the Fig. 2 parts b) and c) were designed to adapt the NACA0012 airfoil to the whole width of the test section of icing wind tunnel facility. Multiple connectors and rods (f and g) are used for positioning and angle of attack adjustment (h) of the NACA0012 airfoil. To prevent accretion on the side parts in order to avoid view blockage from the side camera, additional high powered film heaters (d) are attached that lead to complete run-back and access to accreted ice blocks on the middle insert. To prevent heat transfer from the middle insert to the side parts a thin teflon insulation (e) is attached to either side of the airfoil. if

needed, temperature measurements on the side parts can be obtained using five PT1000 temperature sensors that are embedded on the custom film heaters. The side parts are then assembled together with a thin aluminium sheet using a thermally conductive adhesive which allows for a smooth outer-finish of the heatable target.

To gather quantitative accretion growth data from the NACA0012 airfoil, an optical setup is defined and put in place that allows for quantitative accretion observation from cameras 1 and 2 and qualitative observation from the oblique perspective via camera 3. All three cameras focus the leading edge of the model and produce shadowgraphy videos of the ice accreted on the middle heatable insert from top and side perspective. The bright background for the shadowgraphy were achieved by means of diffuser (sand-blasted glass) placed on the bottom and side windows in line with the cameras and high-powered flicker free light sources. Additionally, for observation of evolution of surface temperature at the leading edge of the NACA0012 airfoil an IR camera is situated close to the bottom window (marked as 4). Fig. 3 illustrates the cross-sectional views of optical and thermal observation perspectives.

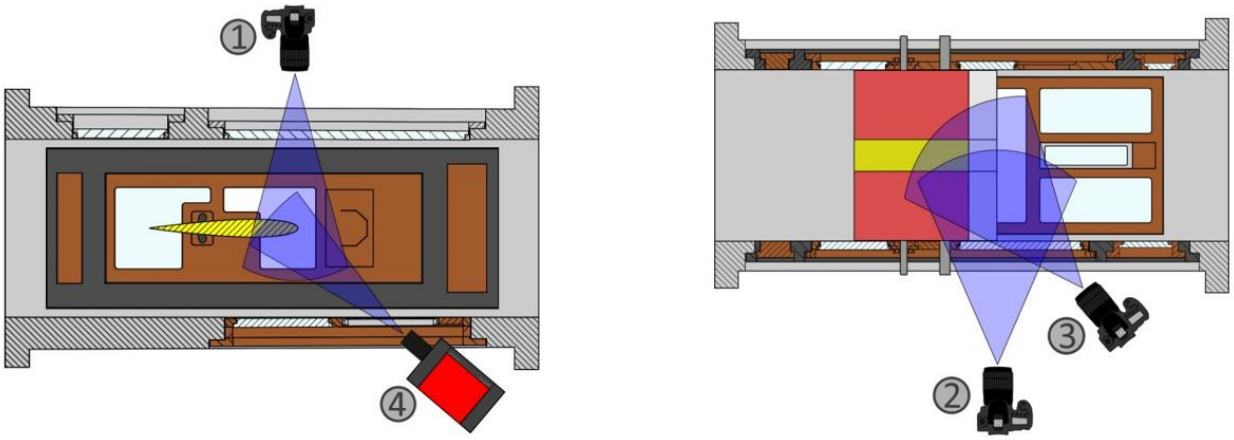

(a) Vertical crosssection (b) Horizontal crosssection

Fig. 3 Cross-sectional Views of the NACA0012 model from Horizontal and Vertical perspective

C. Quantitative Accretion Data using Ice Detection Software

The quantitative ice accretion videos captured by the cameras 1 and 2 were analyzed using an automated Python script developed in [11]. The first frame of each video was used to get a clean plate of the test article leading edge, allowing for easy implementation and future usage of the same script for differently shaped test articles. Due to the high contrast achieved through the shadowgraphy setup and additional post-processing of the videos, a flood fill algorithm was able to identify the contours of the ice accretion very precisely. A comparison between images containing ice accretion and the clean plate of the leading edge allowed for an easy way of detecting the ice accretion, as shown in Figure 4.

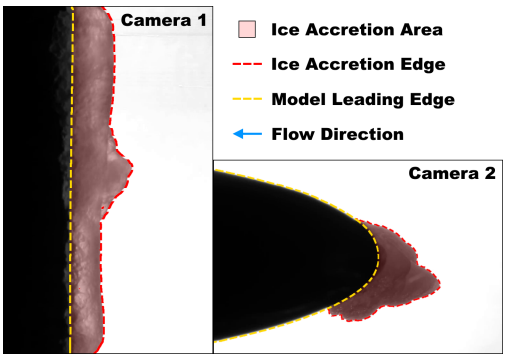

Fig. 4 Ice accretion detected by the ice detection software

The data includes the average and the maximum ice accretion thickness detected by camera 1, as well as the maximum ice accretion thickness and ice accretion cross section area detected by camera 2. The accretion cross section and accretion distribution as viewed from camera 1 are then used to calculate an estimation of the ice accretion volume. Furthermore, the comparison of the maximum accretion thickness measured by camera 1 and 2 provides a basis for parallax error estimation due to a possible misalignment of camera 2 with the leading edge axis, as well as a method of determining whether the view of camera 2 was obstructed by ice accretion on the side parts of the test article. As mentioned in Subsection III.B, this process of identifying cases with obstructed camera 2 videos was aided by the manual evaluation of camera 3 videos.

To achieve a high accuracy with the unit conversion from pixel to mm, multiple calibration photos were taken at the start of each day. The calibration plate was used to calculate the px to mm conversion ratio for the camera 1, as well as the conversion ratios of camera 2 at three different points along the leading edge, as shown in Figure 5. This was used to calculate the conversion ratio for each frame of the videos from camera 2 individually, by applying the calculated perspective distortion from the calibration to the corresponding frame of the camera 1 video and calculating the most probable cross section visible to camera 2.

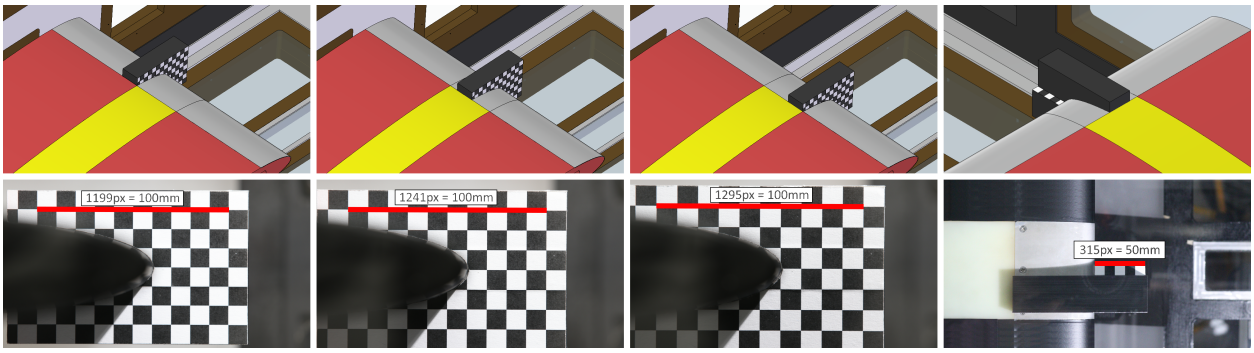

Fig. 5 Calibration plate placement and corresponding calibration pictures

IV. Numerical Method

Based on the observations from the experiments (Sec. V), it seems that the triple deck approach proposed in [12] does not accurately describe what is observed at early times with the formation of a semi frozen layer containing both liquid and solid water on the wall. The superposition of the three layers is replaced here by a single layer characterized by its liquid water volume fraction α_l.

A coupling between the domain (1) composed of the liquid/solid mixture and the domain (2) defined by the solid wall is carried out at $z = 0$ (Fig. 6). Domain (1) extends from $z = 0$ to $z = h$ while domain (2) extends from $z = -l$ to $z = 0$. Heat equation solved inside the wall (domain (2) in Fig. 6) is given by:

$$\frac{\partial}{\partial t}\left(\rho c_p T\right) - \nabla \cdot (\lambda \nabla T) = S \tag{1}$$

where ρ, c_p and λ are respectively the density, the heat capacity and the thermal conductivity of the material (possibly anisotropic) composing the wall. The source term S allows to take into account heating mats which can be embedded into the wall. The boundary conditions are given by:

$$-\lambda \left.\frac{\partial T}{\partial z}\right|_{z=-l} = \Phi_{int} + h_{int}\left(T_{int} - T_{z=-l}\right) \tag{2a}$$

$$\lambda \left.\frac{\partial T}{\partial z}\right|_{z=0} = \Phi_0^+ \tag{2b}$$

Equations (2a) and (2b) respectively stand for the boundary conditions at the bottom of the wall ($z = -l$, Fourier-Robin type) and at the interface with the liquid/solid mixture ($z = 0$, Neumann type). Φ_{int}, h_{int} and T_{int} are prescribed constants. Φ_0^+ is the heat flux transferred by the domain (1) to the domain (2).

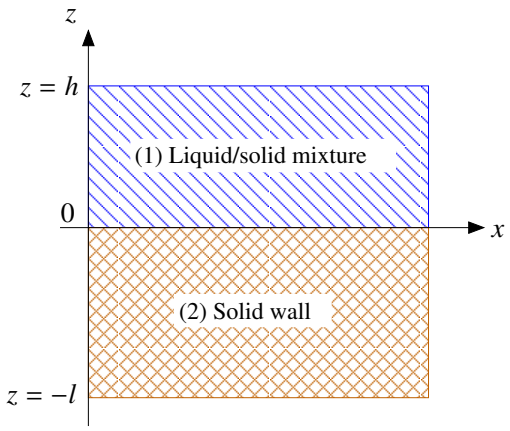

Fig. 6 Coupling between the liquid/solid mixture (domain 1) and the solid wall (domain 2). Domain (1) extends from $z = 0$ to $z = h$ while domain (2) extends from $z = -l$ to $z = 0$.

The equations solved for the liquid/solid mixture (ice accretion in domain (1)) are given by:

$$\frac{\partial}{\partial t}(\rho h) + \nabla \cdot (\rho h \boldsymbol{u}) = \dot{m}_{imp} - \dot{m}_{evs} \tag{3a}$$

$$\begin{aligned}\frac{\partial}{\partial t}(\rho h e) + \nabla \cdot (\rho h e \boldsymbol{u}) = {} & \dot{m}_{imp,l}\left[h_l\left(T_{imp,l}\right) + \frac{u_{imp,l}^2}{2}\right] \\ & + \dot{m}_{imp,s}\left[h_s\left(T_{imp,s}\right) + \frac{u_{imp,s}^2}{2}\right] \\ & - \dot{m}_{evs} h_v(T) \\ & + h_t\left(T_r - T\right) \\ & + \Phi_0^-\end{aligned} \tag{3b}$$

The system of Eqs. (3) can be derived from the 3D equations modeling the total mass conservation (equation for ρ) and total energy conservation (equation for ρe) and by integrating these equations with respect to the z variable. The divergence operator ∇ is defined with respect to the wall surface coordinate system. h is the mixture thickness, $\boldsymbol{u}$ its travel velocity and e its mass energy (or enthalpy since they are very closed for both water and ice). $\dot{m}_{imp,l}$ and $\dot{m}_{imp,s}$ are respectively the mass flow rates for impacting liquid water and solid ice. $\dot{m}_{imp}$ is defined as $\dot{m}_{imp} = \dot{m}_{imp,l} + \dot{m}_{imp,s}$. Mass flow rate for evaporation and sublimation is given by $\dot{m}_{evs}$. Temperatures of the impacting liquid water and solid ice are respectively given by $T_{imp,l}$ and $T_{imp,s}$. The same convention is used for the impacting velocities $u_{imp,l}$ and $u_{imp,s}$. Φ_0^- is the heat flux transferred by the domain (2) to the domain (1). Choosing the solid ice at the melting temperature ($T_m = 273K$) as reference state for the energies, the enthalpies h_s , h_l and h_v for the solid ice, liquid water and steam can be written:

$$h_s(T) = c_{p,s}\left(T - T_m\right) \tag{4a}$$

$$h_l(T) = c_{p,l}\left(T - T_m\right) + L_f\left(T_m\right) \tag{4b}$$

$$h_v(T) = c_{p,l}\left(T - T_m\right) + L_f\left(T_m\right) + L_v(T) \tag{4c}$$

Where $c_{p,l}$ and $c_{p,s}$ are respectively the heat capacities for liquid water and solid ice. The latent heats for melting and vaporization are given by L_f and L_v . In Eq. (3b), the temperature T and the energy e are related by the following relationship:

$$\begin{aligned} T = T_m + \frac{e}{c_{p,s}} \quad & \text{and} \quad \alpha_l = 0 \quad \text{if} \quad e \le 0 \\ T = T_m \quad & \text{and} \quad \alpha_l = \frac{e}{L_f\left(T_m\right)} \quad \text{if} \quad 0 \le \frac{e}{L_f\left(T_m\right)} \le 1 \\ T = T_m + \frac{L_f\left(T_m\right)}{c_{p,l}}\left(\frac{e}{L_f\left(T_m\right)} - 1\right) \quad & \text{and} \quad \alpha_l = 1 \quad \text{if} \quad 1 \le \frac{e}{L_f\left(T_m\right)} \end{aligned} \tag{5}$$

Equations (1) + (2) and (3) are coupled to ensure the continuity of both the temperature T_0 and the heat flux Φ_0 at the interface between the solid/ice mixture and the heated wall ($z = 0$):

$$T_0^+ = T_0^- \tag{6a}$$

$$\Phi_0^+ = -\Phi_0^- \tag{6b}$$

To do this, a coupling procedure derived from [13] is used. To close the coupling, a relationship is needed between T_0^+ and the corresponding average temperature of the ice layer T which is the only available information on the temperature profile in the accretion shape, since Eqs. (3) has been obtained by eliminating the variable z. To do so, a uniform temperature (in the normal-z direction) is assumed in the whole accretion thickness.

The models described in this section have been assessed for the heatable NACA0012 airfoil configuration in ice crystal icing conditions. This is presented in Sec. V.

V. Results and Analysis

The previous models for the solid body and the water layer are used to simulate the heatable NACA0012 airfoil configuration. The simulations are two dimensional. The airfoil is meshed using 10000 triangular elements. In order to reduce the computational cost the internal insulation is not taken into account and is replaced by an adiabatic wall boundary condition as shown in Figure 7.

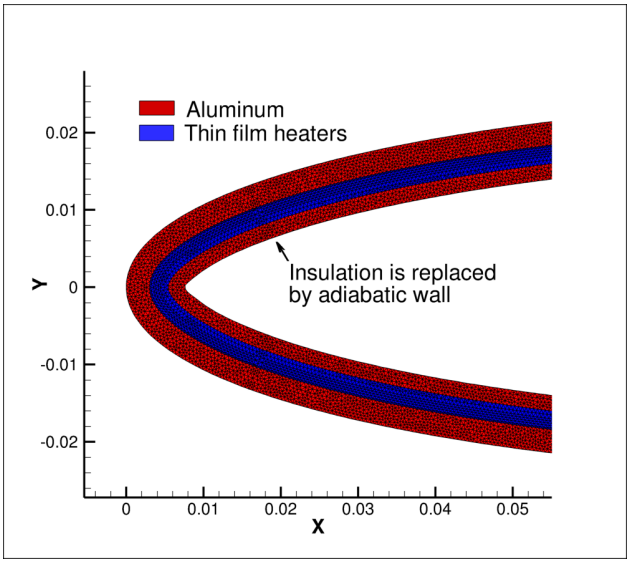

Fig. 7 Mesh of the NACA0012 airfoil and its decomposition into several material subdomains

Several tests from the experimental database where used in order to assess the proposed models and numerical methodology. They are described in Table 1.

-	AoA [°]	U_∞ $[m.s^{-1}]$	T_∞ $[K]$	IWC $[g.m^{-3}]$	Q $[W.m^{-2}]$
Test 01	0	40	267.65	16.2	6200

Table 1 Aerodynamic and icing conditions for simulated tests

Figure 8 shows a comparison between the ice shapes obtained by numerical simulation and experiment. The numerical simulations are able to correctly capture the order of magnitude of the ice thickness at the tip. Nevertheless, the ice thickness is overestimated on the sides. This may be due to an underestimation of the mass loss by erosion.

Additional results, analyses and details will be provided in the final version of the manuscript.

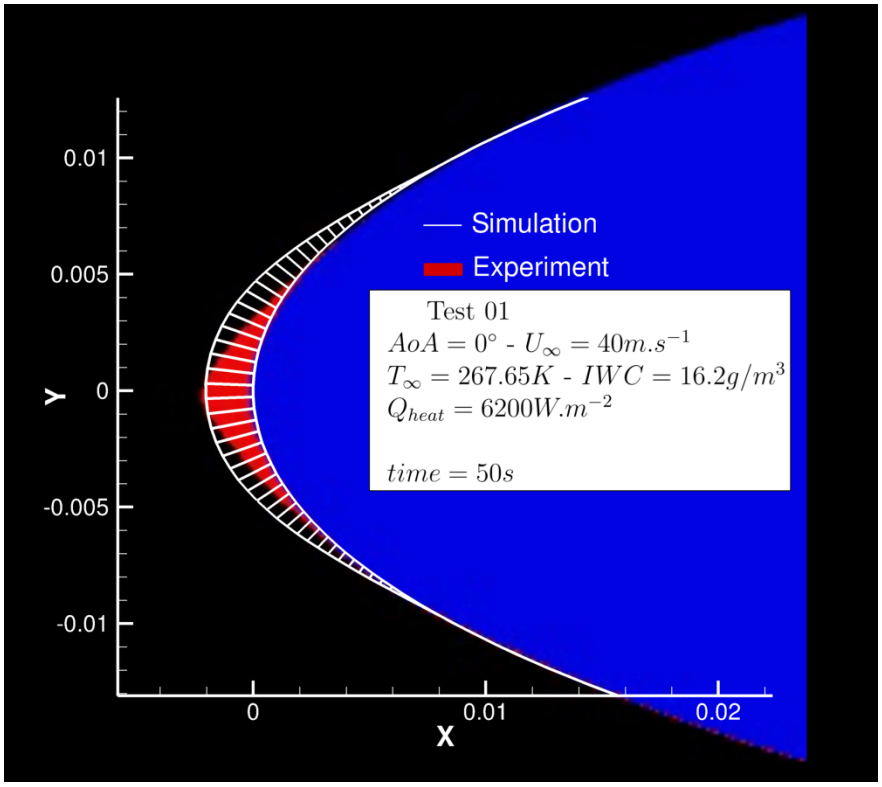

Fig. 8 Test 01: comparison between the ice shapes obtained by simulation and experiment

VI. Conclusion

Conclusion will be shared in the final version of the manuscript.

Appendix

Additional results will be shared in this section of the paper due to be submitted in the final manuscript.

Acknowledgments

This research work is carried out and received funding under the framework of European Union's Horizon 2020 research and innovation programme with grant agreement No. 767560.

The authors would like to express gratitude to Stephan Sattler and Reinhard Kerbstadt for sharing valuable input and expertise on model assembly and electronics. Special thanks to Dan Fuleki from CNRC with regards to sharing technical data for different components used in the assembly of the test article.

References

[1] Gent, R. W., Dart, N. P., and Cansdale, J. T., "Aircraft icing," *Philosophical Transactions of the Royal Society of London. Series A: Mathematical, Physical and Engineering Sciences*, Vol. 358, No. 1776, 2000, pp. 2873–2911.

[2] Werries, M., "Airplane Plus Heat Plus Ice Equals Mystery." 2017.

[3] AGARD, "Agard advisory report 334 - ice accretion simulation," 1997.

[4] Lamb, D., and Verlinde, J., *Physics and chemistry of clouds*, Cambridge University Press, 2011.

[5] Ludlam, F., and Mason, B., "The physics of clouds," *Geophysik II/Geophysics II*, Springer, 1957, pp. 479–540.

[6] Mason, J., "Engine Power Loss in Ice Crystal Conditions," Vol. 04, No. 12, 2007.

[7] Bansmer, S. E., Baumert, A., Sattler, S., Knop, I., Leroy, D., Schwarzenboeck, A., Jurkat-Witschas, T., Voigt, C., Pervier, H., and Esposito, B., "Design, construction and commissioning of the Braunschweig Icing Wind Tunnel," *Atmospheric Measurement Techniques*, Vol. 11, No. 6, 2018, pp. 3221–3249.

[8] Baumert, A., Bansmer, S., Sattler, S., Pervier, H., and Esposito, B., "Simulating natural ice crystal cloud conditions for icing wind tunnel experiments-A review on the design, commissioning and calibration of the TU Braunschweig ice crystal generation system," *8th AIAA Atmospheric and Space Environments Conference*, 2016, p. 4053.

[9] Baumert, A., *Experimental and Numerical Studies on Ice Crystal Icing of Civil Aircraft*, TU Braunschweig-Niedersächsisches Forschungszentrum für Luftfahrt, 2019.

[10] Breiling, M., Bacher, M., Sokratov, S., and Best, F. G., "Method and device for producing snow," , Aug. 30 2016. US Patent 9,429,348.

[11] Vorgias, E. A. J., "Influence of Ice Crystal Properties on Ice Accretion Phenomenon," , 04.2021. TU Braunschweig, Institute for Fluid Mechanics, unpublished Bachelor's Thesis.

[12] Chauvin, R., Bennani, L., Trontin, P., and Villedieu, P., "An implicit time marching Galerkin method for the simulation of icing phenomena with a triple layer model," *Finite Elements in Analysis and Design*, Vol. 150, 2018, pp. 20–33.

[13] Bennani, L., Trontin, P., Chauvin, R., and Villedieu, P., "A non-overlapping optimized Schwarz method for the heat equation with non linear boundary conditions and with applications to de-icing," *Computers & Mathematics with Applications*, Vol. 80, No. 6, 2020, pp. 1500–1522.